Modeling and Numerical Simulation of Material Science, 2022, 12, 1-11
https://www.scirp.org/journal/mnsms
ISSN Online: 2164-5353
ISSN Print: 2164-5345

The Mechanical and Electronic Properties of Ternary Rare-Earth Hexaboride $La_xNd_{8-x}B_6$ (x = 0, 1, 7, 8) Materials

Cengiz Bozada

Department of Metallurgical and Material Science Engineering, Faculty of Engineering, Gaziantep University, Gaziantep, Turkey
Email: b.ankara@yandex.com

How to cite this paper: Bozada, C. (2022) The Mechanical and Electronic Properties of Ternary Rare-Earth Hexaboride $La_xNd_{8-x}B_6$ (x = 0, 1, 7, 8) Materials. *Modeling and Numerical Simulation of Material Science*, **12**, 1-11.
https://doi.org/10.4236/mnsms.2022.121001

Received: January 1, 2022
Accepted: January 27, 2022
Published: January 30, 2022

Abstract

We have carried out density functional theory to study the lattice constants and electronic properties of LaB_6, NdB_6, Nd-doped LaB_6, and La-doped NdB_6. The lattice constant, intra-octahedral bond, inter-octahedral boron bond, and positional parameter (z) were calculated for LaB_6, $La_7Nd_1B_6$, $La_1Nd_7B_6$, and NdB_6. Our results show that the doped Nd increases the lattice constant of $La_7Nd_1B_6$. Likewise, La-doping leads to an increase in the lattice constant of the $La_1Nd_7B_6$. The PDOSs of LaB_6, B of LaB_6, $La_7Nd_1B_6$, B of $La_7Nd_1B_6$, $La_1Nd_7B_6$, B of $La_1Nd_7B_6$, NdB_6, and B of NdB_6 were calculated. La d-electron bands cross the Fermi energy, showing classical conductor behavior. The charge density results indicate that light and dark colors show high and low-intensity zones, respectively. $La_1Nd_7B_6$ has a low-density region and LaB_6 has a high-density region. The LaB_6 midpoint has strong charge density peaks. Weak peaks are also observed for $La_1Nd_7B_6$. Thus, ternary REB_6 has good potential for many applications. This article reports an investigation of the electronic features and structural parameters of binary and ternary hexaborides.

Keywords

Rare-Earth Hexaboride, Lattice Constant, PDOS, Charge Density

1. Introduction

Rare-earth hexaborides (REB_6) are commonly used in various high-energy optical devices and field electron emitter systems because of their superior properties such as high chemical stability, high melting point, high mechanical strength, high brightness, low work function, low volatility, conductibility, small visual dimensions and long lifetimes [1]. REB_6 is commonly used as cathode material.

REB_6 has a cubic CsCl-type structure with a space group of Pm-3m symmetry, in which a rare-earth (RE) ion occupies the Cs site, and the B_6 octahedron is located on the Cl site. REB_6 compounds include LaB_6, CeB_6, PrB_6, NdB_6, PmB_6, SmB_6, EuB_6, GdB_6, TbB_6, DyB_6, HoB_6, ErB_6, TmB_6, YbB_6, LuB_6, ScB_6 and YB_6. LaB_6 has low volatility, CeB_6 indicates a typical dense Kondo behavior, PrB_6 shows high density, NdB_6 has low magnification, SmB_6 is a typical valence semiconductor and GdB_6 has the lowest work function among REB_6 compounds [2].

The electronic structures of the doped and binary REB_6 were calculated using density functional theory (DFT). The position of the Fermi energy level and DOS were adjusted by doping with REB_6 to improve the electron emission characteristics. The high-density d-orbital electrons play a crucial role in considerably decreasing the work function of REB_6 and contributing to the electronic states of electron emission near the Fermi level. This ensures excellent emission characteristics [3]. The second-order elastic constants (SOECs) and third-order elastic constants (TOECs) of LaB_6 and CeB_6 were studied by first-principles calculations. The effect of increased pressure on the elastic anisotropy, mechanical characteristics and structural stability of LaB_6 and CeB_6 has attracted considerable attention. When the pressure increases, the mechanical stability decreases and the ductility and anisotropy increase [1]. Lanthanum hexaborides (LaB_6) are superb thermionic and field electron emission cathode materials in the field of electron emission. LaB_6 has several applications in high-power electronics owing to its long lifetime and high luminosity. LaB_6 attracts attention by its low work function between 2.6 and 2.8 eV, its high melting point of 2715˚C, and its stable chemical and physical characteristics. Compared to polycrystalline and single-crystal applications of LaB_6, it has better potential for single-crystal applications [4]. LaB_6 works well as a thermal-field emitter. It is easily degradable and stable in air. LaB_6 was reactive at 2715˚C. LaB_6 is a violet-colored metal and its electron conductivity is approximately 1/5 that of copper [5]. Lu *et al.* [6] successfully fabricated LaB_6 nanocubes with an average dimension of 94.7 nm using a low-temperature molten salt technique at 800˚C. LaB_6 nanocubes exhibited high near-infrared (NIR) adsorption. As mentioned in [7], LaB_6 nanocrystalline preparation routes include many synthesis routes, such as the floating zone method, aluminum flux, molten salt, high-temperature reaction, chemical vapor deposition (CVD), direct solid-phase reaction and carbothermal reduction. It is because of its wonderful characteristics that LaB_6 is commonly used in some electrical devices, including free-electron laser, thermionic electron cathode, electron microscope, vacuum, and electron beam welder [8].

Neodymium hexaboride (NdB_6) is black solid with good chemical stability, magnetic properties, electrical conductivity, and thermal conductivity characteristic. NdB_6 is insoluble in hydrofluoric acid (HF) and hydrochloric acids (HCl). However, it can be dissolved in molten alkali, sulfuric acid (H_2SO_4) and nitric acid (HNO_3). In addition, it exhibits very high antioxidant capability [9]. NdB_6 crystallizes in a CsCl-type structure with a space group of Pm-3m symmetry, where the neodymium (Nd) occupies the Cs site and octahedral B_6 molecules are

located at the Cl site. NdB_6 has a low work function (1.6 eV) [10]. NdB_6 are an efficient field-emission cathode material. These excellent properties make NdB_6 nanomaterials promising materials for use in vacuum electronic devices [11]. Thus, NdB_6 is antiferromagnetical at T_N = 7.74 K [12]. Ding *et al.* [13] successfully synthesized NdB_6 nanowires (NWs) by a self-catalyst method. Nanowires with diameters of approximately 80 nm and lengths spanning several micrometers have monocrystalline structures. Xu *et al.* [14] successfully produced NdB_6 nanostructures using a free-CVD process. The NdB_6 nanostructures exhibited a good stability. The effect of temperature on NdB_6 is important. When the temperature was increased, the turn-on and threshold electric fields decreased. The work function of NdB_6 nanostructures is considerably decreased as the temperature increases, leading to much enhanced field emission characteristics.

Tsuji *et al.* [15], studied the magnetoresistance, magnetization and specific heat of $Nd_xLa_{1-x}B_6$ (x = 0. 9, 0.8, 0.7, 0) by a FZM method. The magnetoresistance, magnetization and specific heat are affected by temperature. As the temperature increased the others increase. Chaolong *et al.* [16] successfully investigated $Nd_xLa_{1-x}B_6$ bulks using spark plasma sintering (SPS) method. The work function of $Nd_xLa_{1-x}B_6$ was 2.72 eV. The Nd content enhanced thermionic emission characteristic and decreased the work function.

Li *et al.* [17] fabricated successfully high-quality, uniform $La_xNd_{1-x}B_6$ nanowires by catalyst-free CVD technique. $La_xNd_{1-x}B_6$ nanowires exhibit a superb field emission performance. Nanowires are used in optoelectronic devices such as nanoelectronic building blocks and flat panel displays.

2. Materials and Methods

Ab initio material modelling based on DFT was performed quantum espresso software (QE) packages based on modelling the material at nanoscales or on an atomic scale [18]. First-principles calculations were performed using the VASP. [19]. The projector augmented wave (PAW) method and the functional form of the generalized gradient approximation (GGA) of Perdew-Burke-Ernzerhof (PBE) were preferred for exchange. The kinetic energy cut-off of the plane-wave basis set was 500 Ry. The Brillouin zone integration was performed at 3 × 3 × 3 k mesh points using methfessel-paxton smearing with a width of 0.02 Ry. A k-mesh 3 × 3 × 3 was used in the brillouin zone integration with Methfessel-Paxton smearing width of 0.02 Ry. Both LaB_6 and NdB_6 have cubic CsCl-type structures with a space group of Pm-3m symmetry [20].

3. Results and Discussion

The bulk unit cell of REB_6 is simple cubic and is found in the symmetry of the space group Pm-3m. The lattice of NdB_6 can be entirely defined using merely the lattice constant, a, and the positional parameter, z, as indicated in **Figure 1**. The lattice constant, a was 1, intra-octahedral boron bond was 2, and inter-octahedral boron bond was 3.

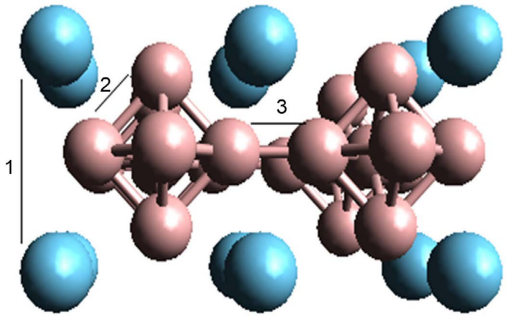

Figure 1. NdB_6 structures with showing relevant bond lengths. NdB_6 contains Nd (blue) and B atoms (purple) forming an octahedral structure.

Table 1 lists the positional parameters of the given REB_6. The lattice constant of LaB_6 (Pm-3m space group) was calculated as a value of 4.157 Å. This was consistent with the experimental consequences indicated in **Table 1**. Furthermore, parameters 2 and 3 were 1.766 and 1.660 Å, respectively, with a boron positional parameter of approximately z = 0.226 Å. Chen *et al.* [28] conducted a study on the structural refinement and thermal expansion of hexaborides. In this study, based on the X-ray powder diffraction technique, the intra-octahedral and inter-octahedral boron–boron distances were calculated as 1.766 and 1.659 Å, respectively. Xiao *et al.* investigated the optical features of LaB_6 using first-principles DFT calculations. They calculated the LaB_6 parameter to be 4.154 Å [33]. Hasan *et al.* [34] synthesized LaB_6 via carbothermal reduction. The calculated value of the lattice parameter was 4.157 Å. Furthermore, other experimental studies [35], [36] are consistent with those of presidential study. Mackinnon *et al.* [37] calculated the lattice constant of LaB_6 using DFT calculations. The calculated boron parameter (z) was 0.225 Å.

The doping of Nd instead of one La atom led to a slight increase in the lattice constant to 0.502 Å. In addition, 2 and 3 parameters were found to be 1.857 and 1.801 Å, respectively, which indicates an increase in these parameters while the z parameter remains nearly the same as that of LaB_6. In a study related to $La_xGd_{1-x}Bd_6$ synthesized by the SPS technique, the doping of Gd into LaB_6 strengthened the lattice parameters of the structure [38]. In a similar study, Chao *et al.* [39] fabricated $La_7Sm_1B_6$ by solid-state technique. Sm doping led to a decrease in the $La_7Sm_1B_6$ lattice.

The 1, 2, 3 and z parameters; 1 of $La_1Nd_7B_6$ were found as 4.449, 1.812, 1.801, and 0.223 Å respectively. Compared to LaB_6, the ratio of Nd/La increased in parameters 1 2, and 3 but the parameter z didn't change considerably. On the other hand, Li *et al.* [17] conducted a study of single-crystal $La_xNd_{1-x}B_6$ nanowires to investigate the field emission performance and characterization. In this study, when Nd-doped into LaB_6, the lattice parameter of $La_xNd_{1-x}B_6$ was decreased. In a similar study, Chao *et al.* [39] produced $La_xSm_{1-x}B_6$ by solid-state reaction. They employed DFT to describe the characteristic of Sm-doped LaB_6. They obtained the lattice parameters of $La_{0.2}Sm_{0.8}B_6$ and $La_{0.4}Sm_{0.6}B_6$ as 4.123 and

Table 1. The lattice constant (1), intra-octahedral boron bond (2), inter-octahedral boron bond (3), and positional parameter (z) of REB6. z = 3/2 × 1.

		1 (Å)	**2** (Å)	**3** (Å)	**z** (Å)
LaB_6	Present study	4.157	1.766	1.660	0.226
	Previous results	4.154 [4], 4.15 [8], 4.156 [21], 4.145 [22], 4.156 [23], 4.155 [24], 4.155 [25], 4.151 [7], 4.158 [26], 4.176 [27]	1.766 [28]	1.659 [28]	
$La_7Nd_1B_6$	Present results	4.267	1.857	1.801	0.227
	Previous results				
$La_1Nd_7B_6$	Present results	4.449	1.812	1.801	0.223
	Previous results				
NdB_6	Present results	4.118	1.750	1.643	0.227
	Previous results	4.125 [29], 4.132 [10], 4.12 [30], 4.1 [14], 4.157 [27], 4.126 [31], 4.128 [32]			

4.128, respectively. Their results showed that doping LaB_6 with Sm decreases the lattice parameter of $La_xSm_{1-x}B_6$. When the La content was doped into BaB_6, the calculated value of the lattice constant of $La_1Ba_7B_6$ was increased [40]. Luo *et al.* [41] studied $La_1Ca_7B_6$ by first-principles calculations. Ca doping provides increases in the lattice strength of $La_1Ca_7B_6$.

The lattice constant of NdB_6 was calculated as a value of 4.118. Ali *et al.* [12] studied the thermoelectric power of NdB_6 by using the floating zone method. They measured the lattice constant was 4.126 Å. In other studies, Ping *et al.* [42] conducted a study of NdB_6 by using the first principle method. The lattice parameter of NdB_6 was calculated as 4.069 Å. Sandeep *et al.* [35] calculated the lattice parameter of NdB_6 (4.157 Å) using the full-potential linearized augmented plane wave (FP-LAPW) technique. Furthermore, parameters 2 and 3 were found to be 1.750 and 1.643 Å, respectively, and the z parameter was 1.643 Å. Mackinnon *et al.* [37] determined the z parameter as 0.226 Å.

Figure 2 illustrated PDOS of $La_xNd_{8-x}B_6$ (x = 0, 1, 7, 8). As explicated in **Figure 2(a)** and **Figure 2(c)** PDOS curves. La d-electron bands show typical conductive behavior as they pass fermi energy. The lowermost conduction bands (CBs) consisted of B s and the uppermost valence bands (VBs) have consisted of B p are indicated in **Figure 2(b)**. La d-electron band passing Fermi energies are shown in **Figure 2(c)**. The calculation converged with great intensity to a metallic ground state at the E_F, at the Fermi level, as shown in the figure. The zone near E_F is contributed mostly by La d states as explicit in **Figure 2(b)** and **Figure 2(c)**. Besides that, E_F is contributed generally by Nd d states as shown in **Figure 2(e)** and **Figure 2(g)**. This is obvious that the energy division of the La d states and Nd d states additives look alike to B 2p additives, which is a signature of hybridization between La d-Nd d - B 2p states.

Figure 3 shows the charge density of LaB_6, $La_7Nd_1B_6$, $La_1Nd_7B_6$ and NdB_6. Light and dark colors show high and low-intensity zones respectively. Dark and light colours indicate low and high-density regions, respectively. $La_1Nd_7B_6$ has a

low-density region and LaB_6 has a high-density region. There are six boron atoms on the plane. The center of the figure was seen the strong B-B bonds. The LaB_6 midpoint has strong charge density peaks. $La_1Nd_7B_6$ has weak peaks.

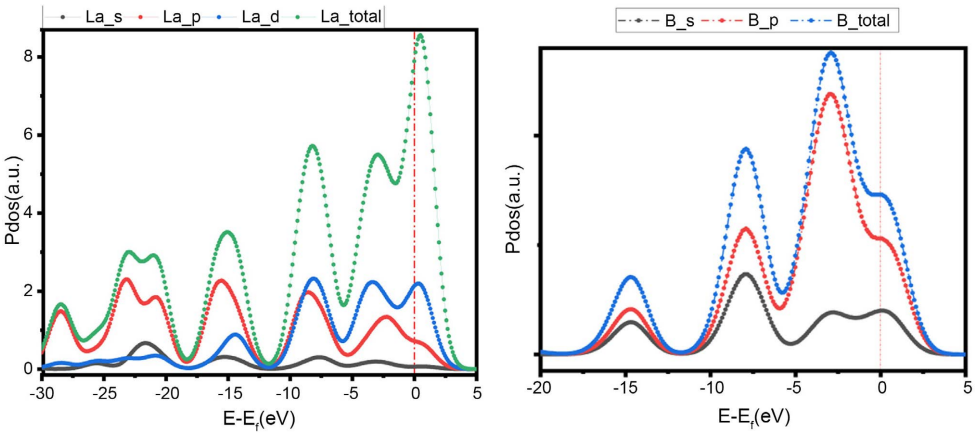

(a) La of LaB_6

(b) B of LaB_6

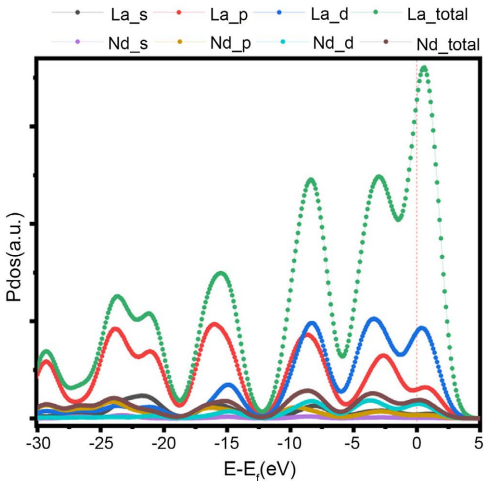

(c) La and Nd of $La_7Nd_1B_6$

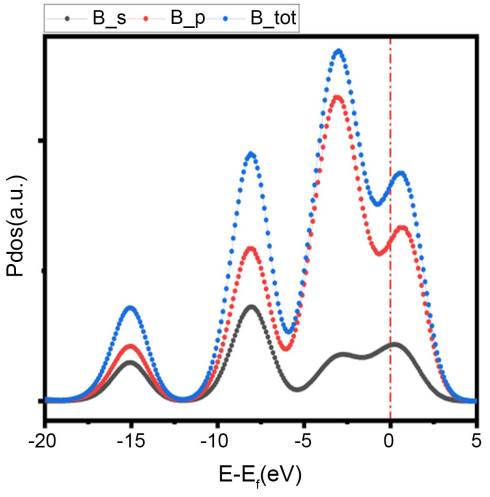

(d) B of $La_7Nd_1B_6$

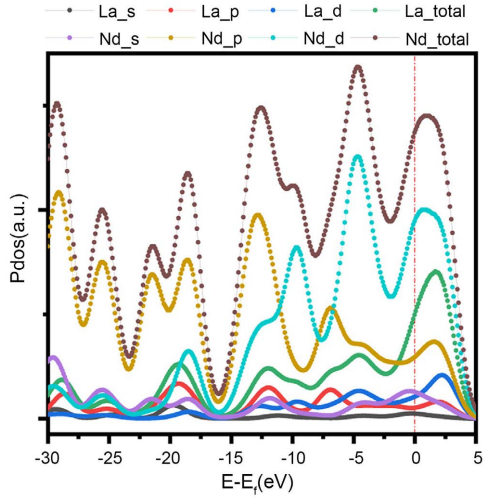

(e) La and Nd of $La_1Nd_7B_6$

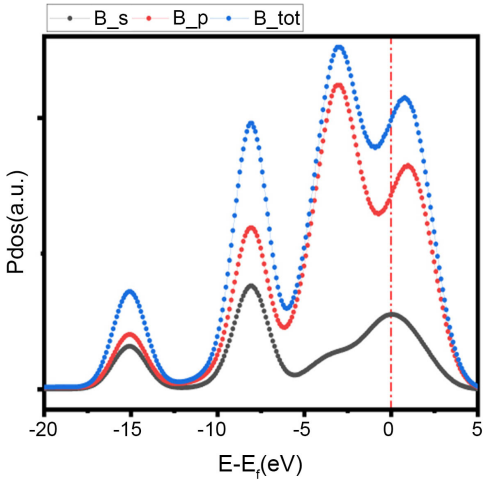

(f) B of $La_1Nd_7B_6$

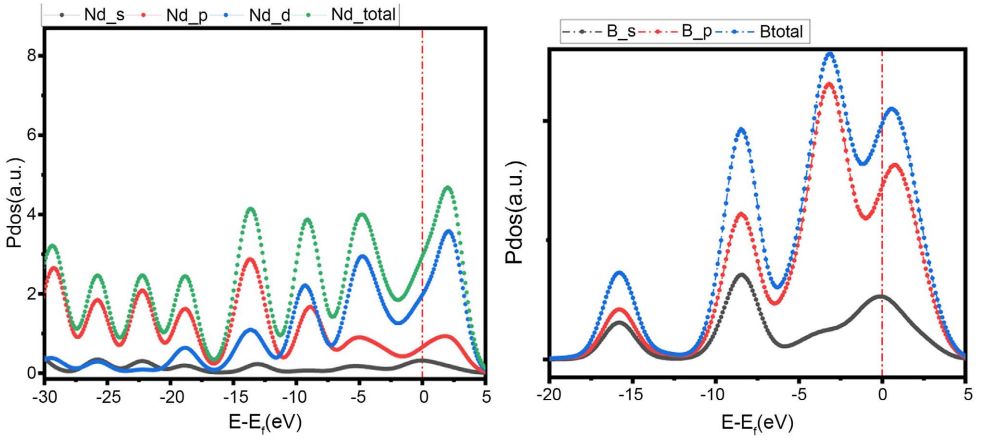

(g) Nd of NdB_6 (h) B of NdB_6

Figure 2. The partial density of states (PDOS) of (a) LaB_6 (b) B of LaB_6 (c) $La_7Nd_1B_6$ (d) B of $La_7Nd_1B_6$ (e) $La_1Nd_7B_6$ (f) B of $La_1Nd_7B_6$ (g) NdB_6 (h) B of NdB_6.

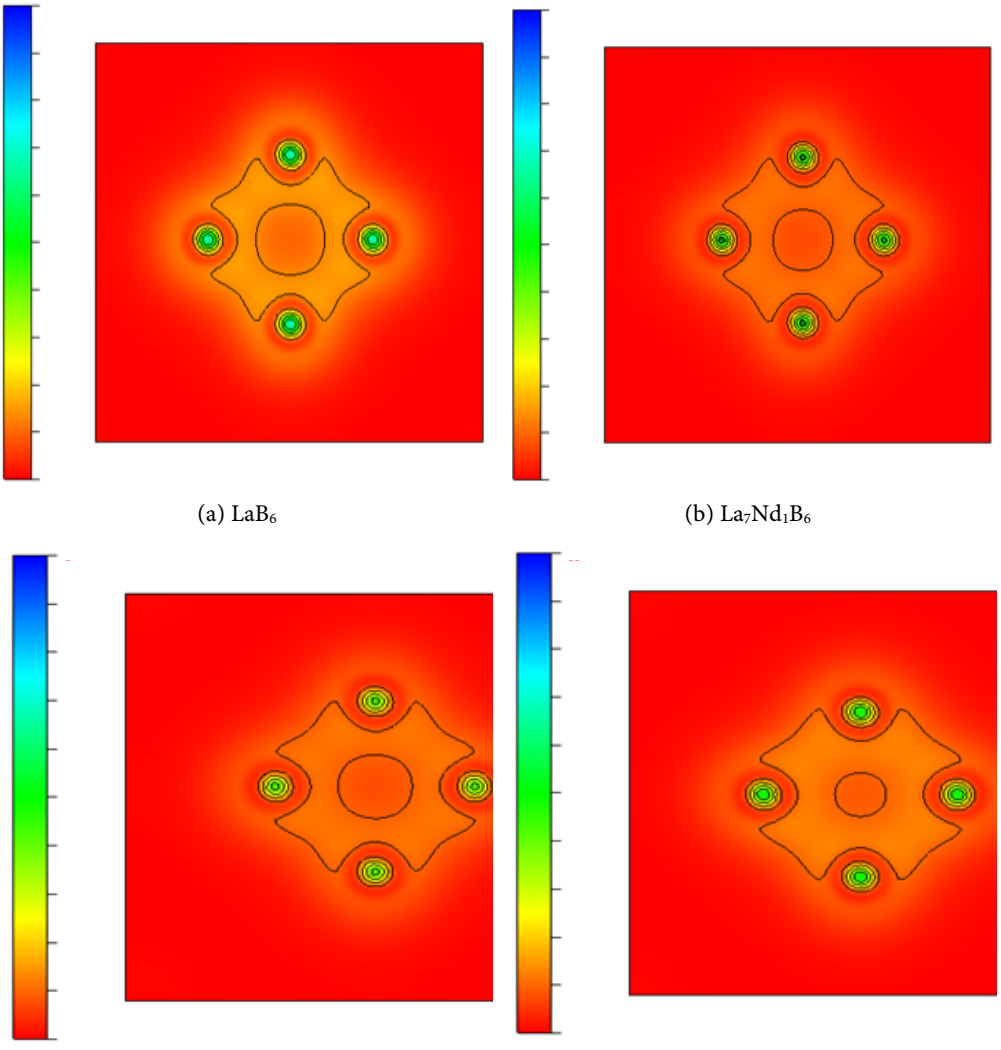

(a) LaB_6 (b) $La_7Nd_1B_6$

(c) $La_1Nd_7B_6$ (d) NdB_6

Figure 3. The charge density of (a) LaB_6 (b) $La_7Nd_1B_6$ (c) $La_1Nd_7B_6$ (d) NdB_6.

4. Conclusion

We comprehensively studied the mechanical and electronic properties of LaB_6, NdB_6, Nd-doped LaB_6 and La-doped NdB_6 using the density functional theory. The lattice constant of LaB_6 was lower than that of Nd-doped LaB_6. In addition, La doping increased the lattice constant of La-doped NdB_6. We calculated the PDOS of LaB_6, B for LaB_6, $La_7Nd_1B_6$, B for $La_7Nd_1B_6$, $La_1Nd_7B_6$, B of $La_1Nd_7B_6$, NdB_6, and B of NdB_6. We found that the La d-electron bands pass the Fermi energy as shown in **Figure 2(c)**. The light color in the charge density indicates that LaB_6 has a high-density region. Similarly, dark color in the charge density shows that $La_1Nd_7B_6$ has a low-density region.

Conflicts of Interest

The author declares no conflicts of interest regarding the publication of this paper.

References

[1] Zeng, X., Ye, Y., Zou, S., Gou, Q., Wen, Y. and Ou, P. (2017) First-Principles Study of the Nonlinear Elasticity of Rare-Earth Hexaborides REB6 (RE = La, Ce). *Crystals*, **7**, 320. https://doi.org/10.3390/cryst7110320

[2] Ji, X.H., Zhang, Q.Y., Xu, J.Q. and Zhao, Y.M. (2011) Rare-Earth Hexaborides Nanostructures: Recent Advances in Materials, Characterization and İnvestigations of Physical Properties. *Progress in Solid State Chemistry*, **39**, 51-69. https://doi.org/10.1016/j.progsolidstchem.2011.04.001

[3] Liu, H., Zhang, X., Xiao, Y. and Zhang, J. (2018) The Electronic Structures and Work Functions of (100) Surface of Typical Binary and Doped REB6 Single Crystals. *Applied Surface Science*, **434**, 613-619. https://doi.org/10.1016/j.apsusc.2017.10.233

[4] Liu, H., Zhang, X., Ning, S., Xiao, Y. and Zhang, J. (2017) The Electronic Structure and Work Functions of Single Crystal LaB_6 Typical Crystal Surfaces. *Vacuum*, **143**, 245-250. https://doi.org/10.1016/j.vacuum.2017.06.029

[5] Uijttewaal, M.A., De Wijs, G.A. and De Groot, R.A. (2006) *Ab İnitio* and Work Function and Surface Energy Anisotropy of LaB_6. *The Journal of Physical Chemistry B*, **110**, 18459-18465. https://doi.org/10.1021/jp063347i

[6] Yu, Y., Wang, S., Li, W., Chen, H. and Chen, Z. (2018) Synthesis of Single-Crystalline Lanthanum Hexaboride Nanocubes by a Low Temperature Molten Salt Method. *Materials Chemistry and Physics*, **207**, 325-329. https://doi.org/10.1016/j.matchemphys.2017.12.081

[7] Zhang, M., *et al.* (2008) A Low-Temperature Route for the Synthesis of Nanocrystalline LaB_6. *Journal of Solid State Chemistry*, **181**, 294-297. https://doi.org/10.1016/j.jssc.2007.12.011

[8] Yu, Y., Wang, S., Li, W. and Chen, Z. (2018) Low Temperature Synthesis of LaB_6 Nanoparticles by a Molten Salt Route. *Powder Technology*, **323**, 203-207. https://doi.org/10.1016/j.powtec.2017.09.049

[9] Dou, Z.-H., *et al.* (2015) A New Method of Preparing NdB6 Ultra-Fine Powders. *Rare Metals*, 1-7. https://doi.org/10.1007/s12598-015-0596-0

[10] Yadav, K.K., Sreekanth, M., Ghosh, S., Ganguli, A.K. and Jha, M. (2020) Excellent

Field Emission from Ultrafine Vertically Aligned Nanorods of NdB6 on Silicon Substrate. *Applied Surface Science*, **526**, Article ID: 146652. https://doi.org/10.1016/j.apsusc.2020.146652

[11] Wang, G., Brewer, J.R., Chan, J.Y., Diercks, D.R. and Cheung, C.L. (2009) Morphological Evolution of Neodymium Boride Nanostructure Growth by Chemical Vapor Deposition. *The Journal of Physical Chemistry C*, **113**, 10446-10451. https://doi.org/10.1021/jp901717h

[12] Ali, N. and Woods, S.B. (1983) Low Temperature Thermoelectric Power of LaB_6, PrB6 and NdB6. *Solid State Communications*, **46**, 33-35. https://doi.org/10.1016/0038-1098(83)90024-8

[13] Ding, Q., Zhao, Y., Xu, J. and Zou, C. (2007) Large-Scale Synthesis of Neodymium Hexaboride Nanowires by Self-Catalyst. *Solid State Communications*, **141**, 53-56. https://doi.org/10.1016/j.ssc.2006.10.001

[14] Xu, J., *et al.* (2013) Excellent Field-Emission Performances of Neodymium Hexaboride (NdB6) Nanoneedles with Ultra-Low Work Functions. *Advanced Functional Materials*, **23**, 5038-5048. https://doi.org/10.1002/adfm201301980

[15] Tsuji, S., Endo, T., Kobayashi, S., Yoshino, Y., Sera, M. and Iga, F. (2002) Rapid Suppression of the Metamagnetic Transition for H 111 in NdB6 by La Doping. *Journal of the Physical Society of Japan*, **71**, 2994-3002. https://doi.org/10.1143/JPSJ.71.2994

[16] Lıang, C.-L., Zhang, X., Zhang, J.-X., Zhang, F.-X. and Wang, Y. (2015) Preparation and Property of $La_{1-x}Nd_xB_6$ Cathode Material. *Journal of Inorganic Materials*, **30**, 363-368. https://doi.org/10.15541/jim20140471

[17] Li, Q., *et al.* (2015) Single-Crystalline $La_xNd_{1-x}B_6$ Nanowires: Synthesis, Characterization and Field Emission Performance. *Journal of Materials Chemistry C*, **3**, 7476-7482. https://doi.org/10.1039/C5TC00804B

[18] Giannozzi, P., *et al.* (2017) Advanced Capabilities for Materials Modelling with Quantum ESPRESSO. *Journal of Physics: Condensed Matter*, **29**, Article ID: 465901. https://doi.org/10.1088/1361-648X/aa8f79

[19] Hobbs, D., Kresse, G. and Hafner, J. (2000) Fully Unconstrained Noncollinear Magnetism within the Projector Augmented-Wave Method. *Physical Review B*, **62**, 11556-11570. https://doi.org/10.1103/PhysRevB.62.11556

[20] Hacker Jr., H. and Lin, M.S. (1968) Magnetic Susceptibility of Neodymium Hexaboride. *Solid State Communications*, **6**, 379-381. https://doi.org/10.1016/0038-1098(68)90161-0

[21] Tekoğlu, E., Ağaoğulları, D., Yürektürk, Y., Bulut, B. and Öveçoğlu, M.L. (2018) Characterization of LaB_6 Particulate-Reinforced Eutectic Al-12.6 wt% Si Composites Fabricated via Mechanical Alloying and Spark Plasma Sintering. *Powder Technology*, **340**, 473-483. https://doi.org/10.1016/j.powtec.2018.09.055

[22] Xiao, Y., Zhang, X., Li, R., Liu, H., Zhou, N. and Zhang, J. (2021) Single-Crystal LaB_6 Field Emission Array is Rapidly Fabricated by Ultraviolet Femtosecond Laser and İts Field Electronic Structure Characteristics. *Vacuum*, **184**, Article ID: 109987. https://doi.org/10.1016/j.vacuum.2020.109987

[23] Soloviova, T.O., Karasevska, O.P., Vleugels, J. and Loboda, P.I. (2021) Thermal Dependent Properties of LaB_6-MeB_2 Eutectic Composites. *Ceramics International*, **47**, 17667-17677. https://doi.org/10.1016/j.ceramint.2021.03.086

[24] Ivashchenko, V.I., Turchi, P.E.A., Shevchenko, V.I., Medukh, N.R., Leszczynski, J. and Gorb, L. (2018) Electronic, Thermodynamics and Mechanical Properties of LaB_6 from First-Principles. *Physica B: Condensed Matter*, **531**, 216-222.

https://doi.org/10.1016/j.physb.2017.12.044

[25] Otani, S., Honma, S., Yajima, Y. and Ishizawa, Y. (1993) Preparation of LaB_6 Single Crystals from a Boron-Rich Molten Zone by the Floating Zone Method. *Journal of Crystal Growth*, **126**, 466-470. https://doi.org/10.1016/0022-0248(93)90052-X

[26] Bai, L., Ma, N. and Liu, F. (2009) Structure and Chemical Bond Characteristics of LaB_6. *Physica B*: *Condensed Matter*, **404**, 4086-4089. https://doi.org/10.1016/j.physb.2009.07.189

[27] Ghimire, M.P., Rai, D.P., Patra, P.K., Mohanty, A.K. and Thapa, R.K. (2012) Study of Bulk Modulus, Volume, Energy, Lattice Parameters and Magnetic Moments in Rare Earth Hexaborides Using Density Functional Theory. *Journal of Physics*: *Conference Series*, **377**, 12084. https://doi.org/10.1088/1742-6596/377/1/012084

[28] Chen, C.-H., Aizawa, T., Iyi, N., Sato, A. and Otani, S. (2004) Structural Refinement and Thermal Expansion of Hexaborides. *Journal of Alloys and Compounds*, **366**, L6-L8. https://doi.org/10.1016/S0925-8388(03)00735-7

[29] Simsek, T., Avar, B., Ozcan, S. and Kalkan, B. (2019) Nano-Sized Neodymium Hexaboride: Room Temperature Mechanochemical Synthesis. *Physica B*: *Condensed Matter*, **570**, 217-223. https://doi.org/10.1016/j.physb.2019.06.047

[30] Han, W., Zhang, H., Chen, J., Zhao, Y., Fan, Q. and Li, Q. (2015) Synthesis of Single-Crystalline NdB 6 Submicroawls via a Simple Flux-Controlled Self-Catalyzed Method. *RSC Advances*, **5**, 12605-12612. https://doi.org/10.1039/C4RA13129K

[31] Blomberg, M.K., Merisalo, M.J., Korsukova, M.M. and Gurin, V.N. (1995) Single-Crystal X-Ray Diffraction Study of NdB6, EuB6 and YbB6. *Journal of Alloys and Compounds*, **217**, 123-127. https://doi.org/10.1016/0925-8388(94)01313-7

[32] Fan, Q.H., *et al.* (2013) Field Emission from One-Dimensional Single-Crystalline NdB_6 Nanowires. *Journal of Rare Earths*, **31**, 145-148. https://doi.org/10.1016/S1002-0721(12)60248-8

[33] Xiao, L., *et al.* (2012) Origins of High Visible Light Transparency and Solar Heat-Shielding Performance in LaB_6. *Applied Physics Letters*, **101**, 41913. https://doi.org/10.1063/1.4733386

[34] Hasan, M., Sugo, H. and Kisi, E. (2013) Low Temperature Carbothermal and Boron Carbide Reduction Synthesis of LaB_6. *Journal of Alloys and Compounds*, **578**, 176-182. https://doi.org/10.1016/j.jallcom.2013.05.008

[35] Sandeep, M.P., Rai, D.P., Patra, P.K., Mohanty, A.K. and Thapa, R.K. (2012) Study of Bulk Modulus, Volume, Energy, Lattice Parameters and Magnetic Moments in Rare Earth Hexaborides Using Density Functional Theory. *Journal of Physics*: *Conference Series*, **377**, 12084. https://doi.org/10.1088/1742-6596/377/1/012084

[36] Hasegawa, A. and Yanase, A. (1977) Energy Bandstructure and Fermi Surface of LaB_6 by a Self-Consistent APW Method. *Journal of Physics F*: *Metal Physics*, **7**, 1245-1260. https://doi.org/10.1088/0305-4608/7/7/023

[37] Mackinnon, I., Alarco, J. and Talbot, P. (2013) Metal Hexaborides with Sc, Ti or Mn. *Modeling and Numerical Simulation of Material Science*, **3**, 158-169. https://doi.org/10.4236/mnsms.2013.34023

[38] Bao, L.-H., Zhang, J.-X., Zhang, N., Li, X.-N. and Zhou, S.-L. (2012) *In Situ* $(La_xGd_{1-x})B_6$ Cathode Materials Prepared by the Spark Plasma Sintering Technique. *Physica Scripta*, **85**, 35710. https://doi.org/10.1088/0031-8949/85/03/035710

[39] Chao, L., Bao, L., Shi, J., Wei, W., Tegus, O. and Zhang, Z. (2015) The Effect of Sm-Doping on Optical Properties of LaB_6 Nanoparticles. *Journal of Alloys and Compounds*, **622**, 618-621. https://doi.org/10.1016/j.jallcom.2014.10.141

[40] Hasan, M.M., Cuskelly, D., Sugo, H. and Kisi, E.H. (2015) Low Temperature Synthesis of Low Thermionic Work Function (La_xBa_{1-x})B_6. *Journal of Alloys and Compounds*, **636**, 67-72. https://doi.org/10.1016/j.jallcom.2015.02.105

[41] Luo, K., *et al.* (2016) Crystal Structures and Mechanical Properties of M (Mg, Sr, Ba, La) x$Ca_{1-x}B_6$ Solid Solution: A First Principles Study. *Ceramics International*, **42**, 6632-6639. https://doi.org/10.1016/j.ceramint.2016.01.002

[42] Qin, P., Xu, C. and Chen, D. (2012) Electronic and Optical Properties of RB_6 (R = La, Nd): A Computer Aided Design. *Advanced Materials Research*, **571**, 239-242. https://doi.org/10.4028/www.scientific.net/AMR.571.239